



**HAL**  
open science

## UV Dust Attenuation in Star-forming Galaxies: II Calibrating the $A(\text{UV})$ vs. $L_{\text{TIR}}/L_{\text{UV}}$ relation

L. Cortese, A. Boselli, P. Franzetti, R. Decarli, G. Gavazzi, Samuel Boissier,  
V. Buat

► **To cite this version:**

L. Cortese, A. Boselli, P. Franzetti, R. Decarli, G. Gavazzi, et al.. UV Dust Attenuation in Star-forming Galaxies: II Calibrating the  $A(\text{UV})$  vs.  $L_{\text{TIR}}/L_{\text{UV}}$  relation. Monthly Notices of the Royal Astronomical Society, 2008, 386, pp.1157. hal-00325441

**HAL Id: hal-00325441**

**<https://hal.science/hal-00325441>**

Submitted on 29 Apr 2021

**HAL** is a multi-disciplinary open access archive for the deposit and dissemination of scientific research documents, whether they are published or not. The documents may come from teaching and research institutions in France or abroad, or from public or private research centers.

L'archive ouverte pluridisciplinaire **HAL**, est destinée au dépôt et à la diffusion de documents scientifiques de niveau recherche, publiés ou non, émanant des établissements d'enseignement et de recherche français ou étrangers, des laboratoires publics ou privés.

# Ultraviolet dust attenuation in star-forming galaxies – II. Calibrating the $A(\text{UV})$ versus $L_{\text{TIR}}/L_{\text{UV}}$ relation

L. Cortese,<sup>1\*</sup> A. Boselli,<sup>2</sup> P. Franzetti,<sup>3</sup> R. Decarli,<sup>4,5</sup> G. Gavazzi,<sup>4</sup> S. Boissier<sup>2</sup>  
and V. Buat<sup>2</sup>

<sup>1</sup>*School of Physics and Astronomy, Cardiff University, Cardiff CF24 3AA*

<sup>2</sup>*Laboratoire d'Astrophysique de Marseille, Traverse du Siphon, BP8 13375 Marseille, France*

<sup>3</sup>*INAF – IASF Milano, via Bassini 15, 20133 Milano, Italy*

<sup>4</sup>*Università degli Studi di Milano-Bicocca, Piazza della Scienza 3, 20126 Milano, Italy*

<sup>5</sup>*Università degli Studi dell'Insubria, via Valleggio 11, 22100 Como, Italy*

Accepted 2008 February 15. Received 2008 February 15; in original form 2007 October 12

## ABSTRACT

We investigate the dependence of the total-IR (TIR) to ultraviolet (UV) luminosity ratio method for calculating the UV dust attenuation  $A(\text{UV})$  from the age of the underlying stellar populations by using a library of spectral energy distributions for galaxies with different star formation histories. Our analysis confirms that the TIR/UV versus  $A(\text{UV})$  relation varies significantly with the age of the underlying stellar population: that is, for the same TIR/UV ratio, systems with low specific star formation rate (SSFR) suffer a lower UV attenuation than starbursts. Using a sample of nearby field and cluster spiral galaxies, we show that the use of a standard (i.e. age-independent) TIR/UV versus  $A(\text{UV})$  relation leads to a systematic overestimate up to 2 mag of the amount of UV dust attenuation suffered by objects with low SSFR and in particular H I-deficient star-forming cluster galaxies. This result points out that the age-independent TIR/UV versus  $A(\text{UV})$  relation cannot be used to study the UV properties of large samples of galaxies including low star-forming systems and passive spirals. Therefore, we give some simple empirical relations from which the UV attenuation can be estimated taking into account its dependence on the age of the stellar populations, providing a less biased view of UV properties of galaxies.

**Key words:** galaxies: evolution – galaxies: fundamental parameters – galaxies: general – ultraviolet: galaxies.

## 1 INTRODUCTION

The use of ultraviolet (UV) emission to shed light on the evolutionary history of galaxies is not straightforward. The presence of dust in galaxies represents one of the major obstacles complicating a direct quantification of the star formation activity in local and high-redshift galaxies. Absorption by dust grains reddens the spectra at short wavelengths completely modifying the spectral energy distribution (SED) of galaxies. Since the UV radiation is preferentially emitted by young stars that are generally more affected by attenuation from surrounding dust clouds than older stellar populations, rest-frame UV observations can lead to incomplete and/or biased reconstructions of the star formation activity and star formation history (SFH) of galaxies affected by dust absorption, unless proper corrections are applied.

Radiative transfer models suggest that the total-IR (TIR) to UV luminosity ratio method (i.e. Buat 1992; Meurer et al. 1995; Xu &

Buat 1995; Meurer, Heckman & Calzetti 1999) is the most-reliable estimator of the dust attenuation in star-forming galaxies, because it is almost completely independent of the extinction mechanisms (i.e. dust/star geometry, extinction law, see Buat & Xu 1996; Meurer et al. 1999; Gordon et al. 2000; Witt & Gordon 2000). This method is based on the assumption that a fraction of photons emitted by newly formed young stars are absorbed by the dust. The dust heats up and subsequently re-emits the energy in the mid-IR (MIR) and far-IR (FIR). The amount of UV attenuation can thus be quantified by means of an energy balance. The reliability of this method has also made the TIR/UV ratio ideal to calibrate empirical methods to correct for dust attenuation when FIR observations are not available, like the well-known TIR/UV– $\beta$  relation (Meurer et al. 1999, where  $\beta$  is the slope of the UV continuum spectrum in the range  $1300 < \lambda < 2600 \text{ \AA}$ ).

Although almost independent of dust-geometry and extinction law, the TIR/UV ratio method unfortunately depends on the age of the underlying stellar populations. In systems with low specific star formation rate (SSFR), the dust heating by old stars becomes important, and only a fraction of the dust emission is related to the

\*E-mail: luca.cortese@astro.cf.ac.uk

UV absorption (Gordon et al. 2000; Kong et al. 2004; Buat et al. 2005).

In the past, this *age effect* has been generally considered negligible since UV observations were available only for active star-forming systems for which the TIR/UV versus  $A(\text{UV})$  can be assumed to be independent of the SFH (Gordon et al. 2000; Witt & Gordon 2000). However, after the launch of the Galaxy Evolution Explorer (*GALEX*, Martin et al. 2005) this may not be the case any more. *GALEX* is delivering to the community an unprecedented amount of UV data on local and high-redshift galaxies covering the whole range of morphologies and star formation histories: from starbursts to passive spirals and elliptical galaxies (e.g. Boselli et al. 2005a,b, 2006; Donas et al. 2007; Gil de Paz et al. 2007).

Can we extend the use of the *standard method* (calibrated on active star-forming galaxies and starbursts) to correct for dust attenuation to the thousands of galaxies detected by *GALEX*? In recent years, various studies have been undertaken to address these issues (i.e. Kong et al. 2004; Burgarella, Buat & Iglesias-Páramo 2005; Cortese et al. 2006; Dale et al. 2007; Gil de Paz et al. 2007; Panuzzo et al. 2007). However, more attention has been always given to the TIR/UV versus  $\beta$  relation than to the TIR/UV versus  $A(\text{UV})$  relation. Kong et al. (2004) suggested that quiescent galaxies deviate from the TIR/UV– $\beta$  relation of starburst galaxies, because they tend to have redder UV spectra at fixed TIR/UV ratio. They interpreted the different behaviour of starbursts and normal galaxies as due to a difference in the star formation histories, proposing that the offset from the starburst TIR/UV– $\beta$  relation can be predicted using the birthrate parameter  $b$  (Kennicutt, Tamblyn & Congdon 1994; i.e. the ratio of the present to the mean past star formation activity).

In this work, we use a different approach, investigating the dependence of the TIR/UV versus  $A(\text{UV})$  relation on the galaxy SFH, to quantify the influence of the age-independent correction on the interpretation of UV observations. We will adopt a very simple dust geometry model and extinction law to show that the use of standard (i.e. age-independent) methods can strongly bias our interpretation of UV properties of local and high-redshift galaxies. The main goal of this paper is to provide the community with some new empirical relations based on observable quantities suitable for deriving dust-attenuation corrections taking into account the *age effect*. More detailed geometries and dust models have been developed in the last decade (e.g. Buat & Xu 1996; Silva et al. 1998; Bianchi et al. 2000; Charlot & Fall 2000; Witt & Gordon 2000; Calzetti 2001; Panuzzo et al. 2003; Piovan, Tantalo & Chiosi 2006). However, since our results do not depend on the geometry or extinction law adopted (as shown in Appendix A), we decided to adopt a very simple approach in order to make our recipes useful for the widest possible range of astrophysical applications.

In Section 2, we present our model and discuss the variation of the TIR/FUV versus  $A(\text{FUV})$  relation with the age of the underlying stellar population. In Section 3, we apply our model to a sample of nearby field and cluster galaxies and in Section 4 we use this sample to test new empirical recipes to determine  $A(\text{FUV})$ . Additional applications of these techniques are discussed in Section 5.

## 2 THE MODEL

In order to investigate the correlation between the UV dust attenuation  $A(\text{UV})$  and the TIR/UV ratio for different stellar populations, we used a library of SEDs obtained using the Bruzual & Charlot population synthesis models (Bruzual & Charlot 2003). We adopted a Salpeter (1955) initial mass function (IMF) and a SFH ‘a la Sandage’

in the formalism used by Gavazzi et al. (2002):

$$\text{SFR}(t, \tau) = \frac{t}{\tau^2} \exp\left(-\frac{t^2}{2\tau^2}\right), \quad (1)$$

where SFR is the star formation rate per unit mass,  $t$  is the age of the galaxy (we assumed  $t = 13$  Gyr at the present epoch) and  $\tau$  is the time at which the star formation rate reaches the highest value over the whole galaxy history: short  $\tau$  correspond to galaxies dominated by old stellar populations while long  $\tau$  correspond to young (i.e. star-forming) galaxies. We investigated a range of  $\tau$  between 0.1 and 25 Gyr, with steps of 0.2 Gyr for  $0.1 < \tau < 10$  Gyr and 0.5 Gyr for  $\tau > 10$  Gyr and metallicities in the range  $0.02 \leq Z \leq 2.5 Z_{\odot}$  in five steps: 0.02, 0.2, 0.4, 1 and  $2.5 Z_{\odot}$ . The library obtained is able to reproduce all the SEDs typically observed in local galaxies (Gavazzi et al. 2002) and it is only a function of  $\tau$ .<sup>1</sup> Similar libraries can be obtained assuming different SFHs (e.g. exponential SFH, see Appendix A).

Each synthetic SED in our library has been reddened using different values of  $A(\text{FUV})$  in the range  $0 < A(\text{FUV}) < 4$  mag, the typical range observed in normal star-forming galaxies (e.g. Buat et al. 2002; Boissier et al. 2007; Gil de Paz et al. 2007). Higher UV attenuations are normally associated with strong starbursts and highly obscured objects which are outside the goal of this work. For each  $A(\text{FUV})$ ,  $A(\lambda)$  (the attenuation at each  $\lambda$ ) has been derived assuming a Large Magellanic Cloud (LMC) extinction curve (Pei 1992):

$$k(\lambda) = \begin{cases} 1.962(\lambda^{-1}) - 0.55 & \text{if } \lambda^{-1} < 4.2 \mu\text{m}^{-1} \\ -375.91 + 231.23(\lambda^{-1}) & \text{if } (\lambda^{-1} > 4.2 \mu\text{m}^{-1} \text{ and} \\ -46.204(\lambda^{-2}) + 3.0721(\lambda^{-3}) & \lambda^{-1} < 5.5 \mu\text{m}^{-1}) \\ 1.694(\lambda^{-1}) - 0.20 & \text{if } \lambda^{-1} > 5.5 \mu\text{m}^{-1} \end{cases} \quad (2)$$

and a simple sandwich model for dust geometry (Boselli, Gavazzi & Sanvito 2003), where a thin layer of dust of thickness  $\zeta$  is embedded in a thick layer of stars:

$$A(\lambda) = -2.5 \log \left( \left[ \frac{1 - \zeta(\lambda)}{2} \right] \left[ 1 + e^{-\tau_{\text{dust}}(\lambda) \sec(i)} \right] + \left[ \frac{\zeta(\lambda)}{\tau_{\text{dust}}(\lambda) \sec(i)} \right] \left[ 1 - e^{-\tau_{\text{dust}}(\lambda) \sec(i)} \right] \right) \text{ (mag)}, \quad (3)$$

where  $i$  is the galaxy inclination,  $\tau_{\text{dust}}(\lambda)$  is the optical depth and the dust to stars scaleheight ratio  $\zeta(\lambda)$  depends on  $\lambda$  (in units of  $\text{\AA}$ ) as (Boselli et al. 2003):

$$\zeta(\lambda) = 1.0867 - 5.501 \times 10^{-5} \lambda. \quad (4)$$

In the case of the FUV band ( $\lambda \sim 1530 \text{\AA}$ ),  $\zeta \sim 1$ . In this case,  $\tau_{\text{dust}}(\text{FUV})$  can be derived by inverting equation (3):

$$\tau_{\text{dust}}(\text{FUV}) = \left[ \frac{1}{\sec(i)} \right] [0.0259 + 1.2002 A(\text{FUV}) + 1.5543 A(\text{FUV})^2 - 0.7409 A(\text{FUV})^3 + 0.2246 A(\text{FUV})^4]. \quad (5)$$

Using the LMC extinction law  $k(\lambda)$ , we then derive

$$\tau_{\text{dust}}(\lambda) = \frac{\tau_{\text{dust}}(\text{FUV}) k(\lambda)}{k(\text{FUV})} \quad (6)$$

<sup>1</sup> Throughout this paper,  $\tau$  will be only used to indicate the shape of the SED and it must not be adopted to quantify the real age of the stellar populations.

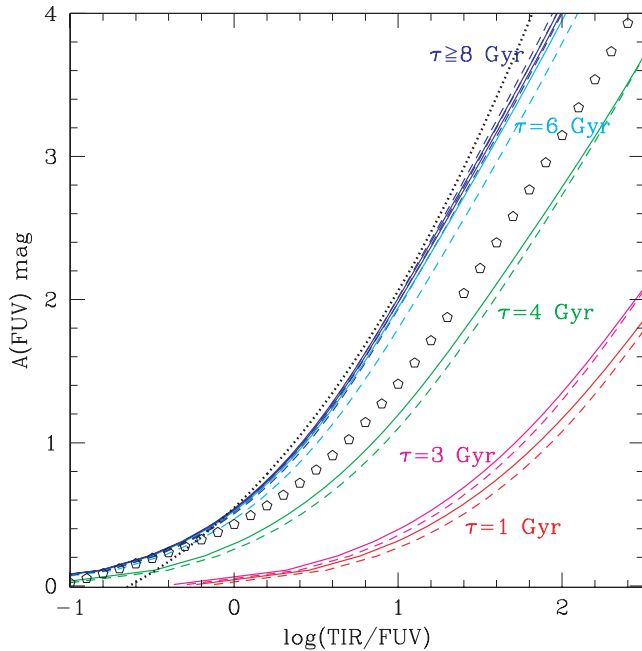


**Figure 1.** The relationship between the TIR/FUV ratio and the FUV attenuation  $A(\text{FUV})$  obtained from our model for different values of  $\tau$ . The solid and dashed lines show the relations for stellar metallicities  $Z = 2.5$  and  $0.02 Z_{\odot}$ , respectively. The dotted black line indicates the age-independent relation given by Buat et al. (2005). The empty pentagons show the relation proposed by Kong et al. (2004) for birthrate parameter  $b \sim 0.06$ .

and compute the complete set of  $A(\lambda)$  using equation (3). In order to simplify the calculations in the following, we assume  $i = 0$ . We adopted the LMC extinction law as a compromise between a Milky Way (MW) extinction law, with a strong bump at  $2175 \text{ \AA}$ , and the Small Magellanic Cloud, with almost no bump at  $\sim 2000 \text{ \AA}$ . Recent analyses have also pointed out that a LMC extinction law can reproduce *GALEX* observations better than a MW or SMC extinction law (Burgarella et al. 2005; Inoue et al. 2006).

The reddened SED is then subtracted from the original *dust-free* SED, providing (once integrated over all wavelengths) the amount of energy absorbed by dust which, assuming an energetic balance, corresponds to the TIR radiation emitted by the galaxy. Finally, by convolving the reddened SED with the *GALEX*-FUV filter we estimated the FUV flux and the TIR/FUV ratio for each model. The relations between  $A(\text{FUV})$  and TIR/FUV so obtained for different values of  $\tau$  and stellar metallicity are shown in Fig. 1.

The mean age of the stellar populations plays a crucial role in the TIR/FUV versus  $A(\text{FUV})$  relation, as already pointed out by several theoretical (e.g. Buat & Xu 1996; Buat & Burgarella 1998; Gordon et al. 2000; Witt & Gordon 2000; Kong et al. 2004; Buat et al. 2005) and observational (e.g. Sauvage & Thuan 1992; Walterbos & Greenawalt 1996; Popescu & Tuffs 2002) studies: for the same TIR/FUV ratio active star-forming galaxies ( $\tau \geq 7 \text{ Gyr}$ ) are more attenuated than objects with low SSFR ( $\tau \sim 4\text{--}5 \text{ Gyr}$ ) or quiescent galaxies ( $\tau \sim 2 \text{ Gyr}$ ). On comparison, we find a very weak dependence ( $< 0.1 \text{ mag}$ ) of the TIR/FUV versus  $A(\text{FUV})$  on stellar metallicity (see Fig. 1). In Table 1, we provide the best polynomial fit (averaged over the whole metallicity range considered) to the  $A(\text{FUV})$  and TIR/FUV for different values of  $\tau$ .

The origin of the *age effect* is clearly visible in Fig. 2 where we compare the amount of the energy absorbed by dust at long ( $\lambda > 4000 \text{ \AA}$ ) and short ( $\lambda < 4000 \text{ \AA}$ ) wavelengths for different values of  $\tau$ . For  $\tau \leq 5 \text{ Gyr}$ , the high-energy photons (mainly UV) contribute to less than the 50 per cent of the total energy absorbed by dust and the FIR emission is mainly due to the re-emission of the stellar radiation emitted by intermediate age stars in the optical. Only for  $\tau \geq 6\text{--}7 \text{ Gyr}$  the UV radiation dominates the dust heating, contributing more than 75 per cent of the whole energy absorbed and re-emitted in the FIR. This also implies that the FIR radiation is not always a good star formation indicator.

We remark that our results do not strongly depend on the parameters adopted in our model (e.g. dust geometry, attenuation law). The variation in the TIR/FUV versus  $A(\text{FUV})$  relations when different attenuation laws are considered is  $\leq 0.2 \text{ mag}$ , as discussed in Appendix A. This is confirmed by the good agreement between our model and the one of Buat et al. (2005) (black dotted line in Fig. 1)

**Table 1.** Relations to convert the TIR/FUV ratio in  $A(\text{FUV})$  for different values of  $\tau$  and FUV – NIR/optical colours.

$\tau$ (Gyr)	$A(\text{FUV}) = (a1) + (a2)x + (a3)x^2 + (a4)x^3 + (a5)x^4$ , where $x = \log(\text{TIR}/\text{FUV})$					FUV – H	FUV – i	FUV – r	FUV – g	FUV – B
	a1	a2	a3	a4	a5					
$\leq 2.6$	0.020 25	0.061 07	0.072 12	0.105 88	–0.015 17	10.5	7.5	7.3	6.7	6.3
2.8	0.023 55	0.069 34	0.087 25	0.103 39	–0.015 26	10.0	7.0	6.9	6.3	5.9
3	0.034 04	0.096 45	0.124 52	0.096 79	–0.015 48	9.6	6.6	6.5	5.9	5.6
3.2	0.058 22	0.155 24	0.178 01	0.086 64	–0.015 93	9.2	6.2	6.1	5.6	5.2
3.4	0.099 44	0.241 60	0.231 61	0.075 80	–0.016 71	8.8	5.9	5.8	5.3	4.9
3.6	0.152 93	0.337 99	0.277 13	0.066 38	–0.017 92	8.4	5.5	5.4	5.0	4.6
3.8	0.209 82	0.429 80	0.314 31	0.059 09	–0.019 57	8.1	5.2	5.1	4.7	4.3
4	0.263 02	0.510 13	0.345 22	0.053 77	–0.021 64	7.8	4.9	4.8	4.4	4.1
4.2	0.308 99	0.577 32	0.371 57	0.050 00	–0.023 99	7.5	4.6	4.6	4.2	3.8
4.4	0.346 95	0.632 24	0.394 38	0.047 39	–0.026 50	7.2	4.3	4.3	3.9	3.6
4.6	0.377 60	0.676 74	0.414 20	0.045 55	–0.029 00	6.9	4.1	4.0	3.7	3.3
4.8	0.402 10	0.712 72	0.431 39	0.044 26	–0.031 40	6.6	3.8	3.8	3.5	3.1
5	0.421 68	0.741 91	0.446 24	0.043 32	–0.033 62	6.3	3.6	3.6	3.3	2.9
5.4	0.450 13	0.785 36	0.470 09	0.042 10	–0.037 45	5.8	3.1	3.1	2.9	2.5
5.8	0.469 09	0.815 20	0.487 87	0.041 38	–0.040 50	5.4	2.7	2.7	2.5	2.1
6.2	0.482 23	0.836 42	0.501 27	0.040 92	–0.042 88	5.0	2.3	2.3	2.1	1.8
6.6	0.491 67	0.852 01	0.511 52	0.040 60	–0.044 75	4.6	1.9	2.0	1.8	1.5
7	0.498 67	0.863 77	0.519 52	0.040 38	–0.046 24	4.2	1.6	1.6	1.5	1.1
$\geq 8$	0.509 94	0.883 11	0.533 15	0.040 04	–0.048 83	$< 4.0$	$< 1.2$	$< 1.3$	$< 1.2$	$< 1.0$

*Note.* Each value of  $\tau$  has been converted into FUV – NIR/optical colours using the relations presented in Table 2.

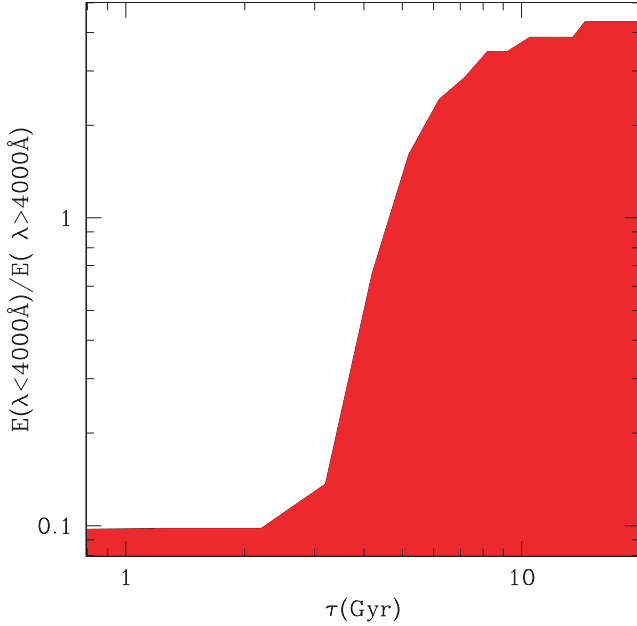


**Figure 2.** The importance of the UV emission in the dust heating. The ratio of the energy absorbed by dust at  $\lambda < 4000$  and at  $\lambda > 4000$  is shown as a function of  $\tau$  (i.e. the age of the Universe at which the galaxy SFR peaks).

in the case of strong star-forming systems and starburst galaxies ( $\tau \geq 8$  Gyr). Our results are also independent of the shape of the adopted SFH and galaxy age. In fact, the TIR/FUV versus  $A(\text{FUV})$  relation mainly depends on the specific star formation and, for the same specific star formation activity, it is not strongly affected by the real shape of the past SFH (see Appendix A). Moreover, in Fig. 1 we show the TIR/FUV versus  $A(\text{FUV})$  relation proposed by Kong et al. (2004) (empty pentagons) for a birthrate parameter  $b \sim 0.06$  (the lowest birthrate parameter considered in their model, corresponding to  $\tau \sim 4.1$  Gyr in our formalism). The level of agreement ( $\sim 0.2$  mag) between Kong et al. (2004) and our model is quite comforting, considering that the Kong et al. (2004) model is based on different SFH (i.e. exponential + bursty model) and geometry (i.e. the time-dependent scenario proposed by Charlot & Fall 2000).

As already discussed by Gordon et al. (2000), the flux ratio method would not be applicable in the case of an embedded starburst in a galaxy with a second older, less-embedded stellar population. At UV and IR wavelengths, the starburst would dominate, but at optical and near-IR (NIR) wavelengths the older population would dominate. However, at least for spiral galaxies in the local Universe this seems not to be the case (Iglesias-Páramo et al. 2004) and smooth SFH like an ‘a la Sandage’ and an exponential well reproduce the observations (e.g. Boselli et al. 2001; Gavazzi et al. 2002; Heavens et al. 2004; Panter et al. 2007). We therefore conclude that our results are model-independent within 0.2 mag (see Appendix A).

### 3 APPLICATION TO NORMAL STAR-FORMING GALAXIES

In order to quantify the impact of the *age effect* on the estimate of the UV attenuation, we computed  $A(\text{FUV})$  for a sample of spiral galaxies and compared our estimate with the one obtained using the standard relation calibrated on active star-forming galaxies (e.g.  $\tau \geq 8$  Gyr,  $\text{FUV} - H \leq 4$  mag,  $b \geq 0.5$ ).

#### 3.1 The data

The sample here adopted is an extension of the optically selected sample described in Cortese et al. (2006), composed by late-type galaxies (later than S0a) including giant and dwarf systems extracted from the Virgo Cluster Catalogue (Binggeli, Sandage & Tammann 1985) and from the CGCG catalogue (Zwicky, Herzog & Wild 1961). The data include galaxies in the Virgo, Abell1367 and Abell262 clusters and part of the Coma–A1367 supercluster (including cluster and field galaxies) observed as part of the All-sky Imaging Survey (AIS) and of the Nearby Galaxy Survey (NGS) carried out by *GALEX* in two UV bands: FUV ( $\lambda_{\text{eff}} = 1530$  Å,  $\Delta\lambda = 400$  Å) and NUV ( $\lambda_{\text{eff}} = 2310$  Å,  $\Delta\lambda = 1000$  Å). We include in our analysis only late-type galaxies detected in both NUV and FUV *GALEX* bands and in both 60- and 100- $\mu\text{m}$  *IRAS* bands: 191 galaxies in total ( $\sim 70$  per cent in high density environments). UV and FIR data have been combined with multifrequency data available. These are optical and NIR H imaging (Gavazzi et al. 2000; Boselli et al. 2003), most of which are available from the GOLDMine galaxy data base (Gavazzi et al. 2003) (<http://goldmine.mib.infn.it>). Data from UV to NIR have been corrected for Galactic extinction according to Burstein & Heiles (1982).

We assume a distance of 17 Mpc for the members of Virgo Cluster A, 22 Mpc for Virgo Cluster B, and 32 Mpc for objects in the M and W clouds (Gavazzi et al. 1999). Members of the Cancer, A1367 and Coma clusters are assumed to lie at distances of 65.2, 91.3 and 96 Mpc, respectively. Isolated galaxies in the Coma supercluster are assumed at their redshift distance, adopting  $H_0 = 75 \text{ km s}^{-1} \text{ Mpc}^{-1}$ .

#### 3.2 SED-fitting technique

The FUV attenuation of each galaxy in our sample has been computed using the following SED-fitting procedure, implemented into the Galaxy Observed Simulated SED Interactive Program (GOSSIP, Franzetti 2005; Franzetti et al. 2008). In order to take into account the *age effect*, we reddened each synthetic SED and fit them to the observed FUV-to-NIR SED obtained using all the available photometric magnitudes.

In details, for each galaxy we compute the observed TIR/FUV ratio using *IRAS* and *GALEX* observations. The TIR flux emitted in the range 1–1000  $\mu\text{m}$  is obtained following Dale et al. (2001):

$$\begin{aligned} \log(f_{\text{TIR}}) = & \log(f_{\text{FIR}}) + 0.2738 - 0.0282 \log\left(\frac{f_{60}}{f_{100}}\right) \\ & + 0.7281 \log\left(\frac{f_{60}}{f_{100}}\right)^2 + 0.6208 \log\left(\frac{f_{60}}{f_{100}}\right)^3 \\ & + 0.9118 \log\left(\frac{f_{60}}{f_{100}}\right)^4, \end{aligned} \quad (7)$$

where  $f_{\text{FIR}}$  is the FIR flux, defined as the flux between 42 and 122  $\mu\text{m}$  (Helou et al. 1988):

$$f_{\text{FIR}} = 1.26(2.58f_{60} + f_{100}) \times 10^{-14} \text{ (W m}^{-2}\text{)} \quad (8)$$

and  $f_{60}$  and  $f_{100}$  are the *IRAS* flux densities measured at 60 and 100  $\mu\text{m}$  (in Jansky). Using the relations presented in the previous section, we then convert the observed TIR/FUV ratio into  $A(\text{FUV})$  for each value of  $\tau$  and  $Z$  considered in our model and determine  $A(\lambda)$  as described in Section 2. Each Bruzual & Charlot (2003) SED is then reddened with the  $A(\lambda)$  obtained following this procedure and fitted to the observed (i.e. not corrected for internal extinction) SED, using a  $\chi^2$  fitting technique similar to the one described in Gavazzi

et al. (2002) and assuming a conservative photometric error of 0.15 mag for each band.

For each galaxy, the value of  $\chi^2$  determines the weight of a given model [as  $\exp(-\chi^2/2)$ ] and a probability distribution function (PDF) for  $\tau$  can be built by combining weights for each model. We then normalize the final PDFs and use the peak value (i.e. the most probable one) as the best estimate of  $\tau$  and the range of  $\tau$  containing 68.2 per cent of the PDF's area (equivalent to the use of constant  $\chi^2$  contours) as estimate of the  $1\sigma$  error. The SED fitting provides not only the best value of  $\tau$  but also the right estimate of  $A(\text{FUV})$  and its uncertainty. The combined use of the observed TIR/FUV ratio for each galaxy and of the relations presented in the previous section makes this method ideal to estimate the UV attenuation for a wide range of morphological types and star formation histories.

### 3.3 The impact of the SFH on the estimate of $A(\text{FUV})$

The difference between the FUV attenuation obtained with the SED-fitting technique ( $A(\text{FUV})_{\text{SED}}$ ) and the one obtained by blindly applying a constant conversion calibrated on star-forming galaxies and starbursts [ $\tau \geq 8$  Gyr,  $A(\text{FUV})_{\text{SB}}$  consistent with the one presented by Buat et al. 2005] is shown in Fig. 3 as a function of  $\tau$  [for clarity only the errors on  $A(\text{FUV})$  are shown]. As already shown in Fig. 1, for low values of  $\tau$  the standard conversion overestimate the UV dust attenuation: in particular for  $\sim 30$  per cent (59/191 galaxies) of our sample the use of a constant TIR/FUV versus  $A(\text{FUV})$  relation leads to an overestimate of more than 0.5 mag of the UV attenuation and for  $\sim 16$  per cent this systematic error exceeds 1 mag. In order to investigate the properties of the most-deviating objects

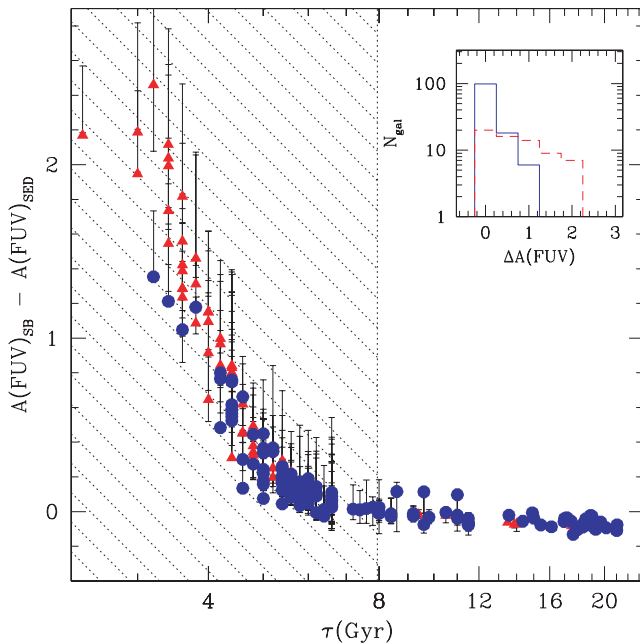


**Figure 3.** The difference between the FUV attenuation for active star-forming galaxies ( $\tau \geq 8$  Gyr; consistent with Buat et al. 2005) and the one obtained from our SED-fitting technique as a function of  $\tau$ . The circles indicate healthy spirals ( $\text{H I-DEF} < 0.4$ ) and the triangles indicate H I-deficient star-forming objects ( $\text{H I-DEF} \geq 0.4$ ). The distributions of the difference for healthy (solid histogram) and deficient (dashed histogram) spirals are shown in the upper right-hand panel. The unshaded area indicates the range of  $\tau$  on which the standard TIR/FUV versus  $A(\text{FUV})$  relation for star-forming galaxies is usually calibrated.

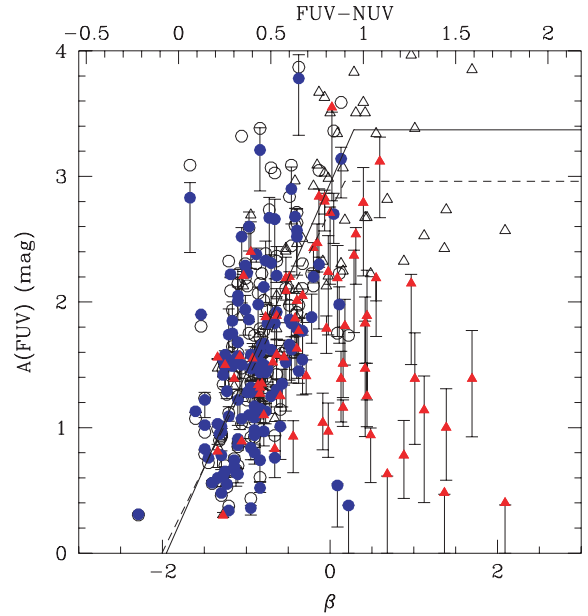


**Figure 4.** The  $A(\text{FUV})$  versus  $\beta$  relation for our optically selected sample.  $A(\text{FUV})$  is computed from our SED-fitting technique (filled symbols) and using the standard recipe for active star-forming galaxies (empty symbols). The solid and dashed lines indicate the relations between  $A(\text{FUV})$  and  $\text{FUV} - \text{NUV}$  proposed by Salim et al. (2007). The symbols are the same as in Fig. 3.

in Fig. 3, we divide our sample according to their H I-deficiency:<sup>2</sup> a value of  $\text{H I-DEF} = 0.4$  has been used to separate healthy (blue circles) from H I-deficient star-forming spirals (red triangles). H I-deficient spirals are among the most-deviating objects in Fig. 3, consistent with the fact that gas deficient objects have normally a SSFR significantly lower than that expected from their luminosity (Boselli et al. 2001). However, also some healthy spirals show a significant offset from the *age-independent* TIR/FUV versus  $A(\text{FUV})$  relation. These are massive early-type spirals with low SSFR, similar to M31 in the Local Group (i.e.  $\text{FUV} - H \sim 7$  mag, Gil de Paz et al. 2007).

The TIR/FUV ratio cannot thus be considered as a good proxy of the UV attenuation for sample of galaxies spanning a wide range of SSFR, in particular in clusters, and relations like the TIR/UV- $\beta$  relation (Meurer et al. 1999; Kong et al. 2004) cannot be blindly used to determine  $A(\text{FUV})$ . This is shown in Fig. 4 where we compare the  $A(\text{FUV})$  versus  $\beta$  relation obtained from our SED-fitting technique (filled symbols) with the one obtained when  $A(\text{FUV})$  is computed using the  $A(\text{FUV})$  versus TIR/FUV relation for strong star-forming galaxies (empty symbols). The  $\beta$  parameter has been computed from the  $\text{FUV} - \text{NUV}$  colour following Kong et al. (2004):  $\beta = 2.201(\text{FUV} - \text{NUV}) - 1.804$ . Galaxies with  $\beta > -0.2$  ( $\text{FUV} - \text{NUV} > 0.75$ ) are mainly H I-deficient galaxies and have a FUV dust attenuation  $\sim 2$  mag lower than the one obtained using the standard  $A(\text{FUV})$ - $\beta$  relation: a difference significantly larger than the typical error on the estimate of  $A(\text{FUV})$  ( $\leq 0.5$  mag) by our fitting technique. The systematic errors introduced in the data are similar

<sup>2</sup> The H I deficiency is defined as the difference, in logarithmic units, between the observed H I mass and the value expected from an isolated galaxy with the same morphological type  $T$  and optical linear diameter  $D$ :  $\text{H I-DEF} = (\log M_{\text{H I}}(T^{\text{obs}}, D_{\text{opt}}^{\text{obs}}) - \log M_{\text{H I}}^{\text{obs}})$  (Haynes & Giovanelli 1984).

when the TIR/FUV ratio is not available and  $A(\text{FUV})$  is determined using empirical methods based on the FUV – NUV colour like the one proposed by Salim et al. (2007), and once again calibrated on strong star-forming galaxies (solid and dashed lines in Fig. 4): for  $\beta > -0.2$ , a UV attenuation in the range  $2.99 < A(\text{FUV}) < 3.32$  mag is predicted, whereas our method gives an average value of  $A(\text{FUV}) \sim 1$  mag. This is mainly due to the fact that in low star-forming systems the UV spectral slope is strongly contaminated by the old stellar populations, whose contribution increases the value of  $\beta$  even if the FUV attenuation is low. This result is consistent with the recent analysis of a sample of  $\sim 1000$  galaxies selected from SDSS presented by Johnson et al. (2007a,b), who found that a large fraction of galaxies having red FUV – NUV colours are also characterized by large 4000-Å break [ $D(4000)$ ], suggesting that part of the dust heating comes from old stellar populations and not from extremely obscured star-forming regions. We can therefore conclude that the TIR/UV- $\beta$  relation can be blindly used to estimate  $A(\text{FUV})$  only for  $\beta < -0.2$  (FUV – NUV < 0.75).

#### 4 OPTIMIZED $A(\text{FUV})$ DETERMINATION: RECOMMENDED METHODS

It clearly appears that a correct estimate of the UV attenuation requires information about the shape of the galaxy SED. A SED-fitting technique like the one described here represents therefore the best method available to quantify  $A(\text{FUV})$  and properly correct UV observations. Unfortunately, SED fitting is only possible when large multiwavelength data sets are available, which is not always the case. For this reason, we investigated the possibility to derive different techniques which can be used to estimate  $A(\text{FUV})$  when SED fitting is not possible. Ideally, these techniques will have a small rms and not display the systematic shift relative to the galaxy age observed in Fig. 3.

The crucial step is to find a good proxy for  $\tau$  (and therefore the shape of the SED). This is particularly important for  $\tau < 6-7$  Gyr where the TIR/FUV versus  $A(\text{FUV})$  relation strongly depends on the age of the stellar populations. The first natural choice is to look for a colour with the largest possible dynamical range, sensitive to small changes in the shape of the SED (Gavazzi et al. 2002). Therefore, in Fig. 5 we plot the distribution of  $\tau$  for our sample as a function of the observed (i.e. not corrected for internal extinction) FUV –  $H$  colour. For  $\tau > 7$  Gyr, the two variables are not correlated and galaxies show approximately the same FUV –  $H$  colour independently of the value of  $\tau$ , reflecting the large error on the estimate of  $\tau$ . This is as expected since in young stellar populations ( $\tau > 7$  Gyr) the variations in the observed FUV –  $H$  colour are mainly due to dust attenuation and not due to age. However, for  $\tau \leq 7$  Gyr (i.e. the range in which we are interested) the FUV –  $H$  is a very good proxy for  $\tau$  (Pearson correlation coefficient  $r \sim -0.91$ ). A simple least-square fitting gives us

$$\log(\tau) = -0.068(\text{FUV} - H) + 1.13 \quad (9)$$

which can be used to estimate  $\tau$  from the FUV –  $H$  colour. The dispersion on this relation varies quite remarkably with the colour. We therefore determine the typical dispersion within 0.5 mag wide FUV –  $H$  bins by combining the  $\tau$ 's PDF for each galaxy in the bin and estimating the  $1\sigma$  error as described in the previous section. The dispersion in the relation (indicated by the shaded area in Fig. 5) is  $\Delta[\log(\tau)] \sim 0.12-0.15$  for  $6 < \text{FUV} - H < 9$  mag, increasing significantly [up to  $\Delta(\log(\tau)) \sim 1$ ] for redder or bluer colours. Similar relations are found when we consider different FUV – optical

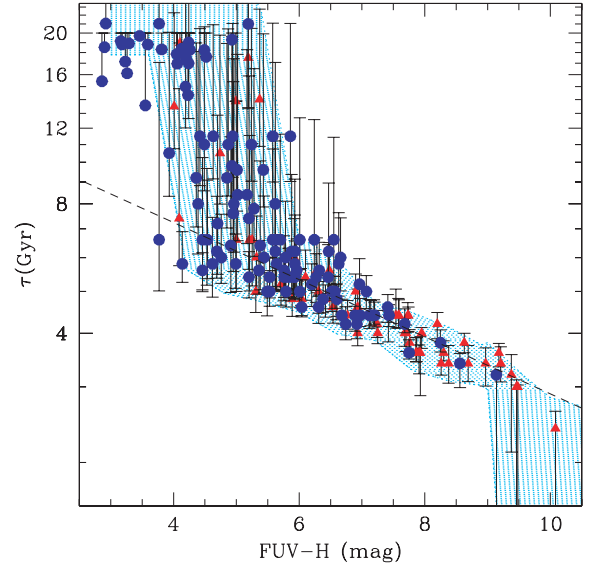


**Figure 5.** Relation between the observed (i.e. not corrected for internal extinction) FUV –  $H$  colour and  $\tau$  for our sample. The dotted line indicates the best linear fit for galaxies having  $\tau \leq 7$  Gyr. The shaded area indicates the typical dispersion of the data computed in FUV –  $H$  bins 0.5 mag wide. The symbols are as in Fig. 3.

**Table 2.** Linear relations useful to estimate  $\tau$  from observed (i.e. not corrected for dust attenuation) FUV – NIR/optical colours [ $\log(\tau) = ax + b$ ]. These relations have been calibrated in the range  $2 \leq \tau \leq 7$  Gyr.

$x$	$a$	$b$	$r$	Validity range
FUV – $H$	-0.068	1.13	-0.91	$4.5 \lesssim \text{FUV} - H$
FUV – $i$	-0.073	0.96	-0.91	$1.6 \lesssim \text{FUV} - i$
FUV – $r$	-0.076	0.97	-0.91	$1.6 \lesssim \text{FUV} - r$
FUV – $g$	-0.083	0.97	-0.91	$1.5 \lesssim \text{FUV} - g$
FUV – $B$	-0.083	0.94	-0.91	$1.1 \lesssim \text{FUV} - B$

colours and are presented in Table 2. We therefore propose two different ways to determine  $A(\text{FUV})$  depending on whether or not FIR observations are available.<sup>3</sup> In Appendix B, we also provide similar recipes in order to determine  $A(\text{NUV})$  in the case FUV observations are not available.

(i) *FIR observations are available.* In this case, we determine the observed TIR/FUV ratio and use one of the relations presented in Table 2 to determine  $\tau$ . Finally, we use the value of  $\tau$  so obtained to choose the conversion between the TIR/FUV ratio and  $A(\text{FUV})$  from the relations provided in Table 1. As discussed above we suggest using the colour covering the widest possible dynamical range, that is, first choice FUV –  $H$ , last choice FUV –  $g$ . The error on the estimate of the FUV dust attenuation [ $\sigma(A(\text{FUV}))$ ] obtained with this method depends on the observational errors on the FUV – optical/NIR colour and on the intrinsic dispersion of the colour- $\tau$  relation adopted. In order to estimate  $\sigma(A(\text{FUV}))$ , for each galaxy in our sample, we generated 1000 random galaxies having FUV –  $H$  colour following a Gaussian distribution centred on the observed colour with  $\sigma = 0.2$  mag (more accurate estimate of the FUV –  $H$

<sup>3</sup> A detailed guide to the recipes presented in this paper can also be found at <http://www.astro.cf.ac.uk/pub/Luca.Cortese/UVattenuation.html>.

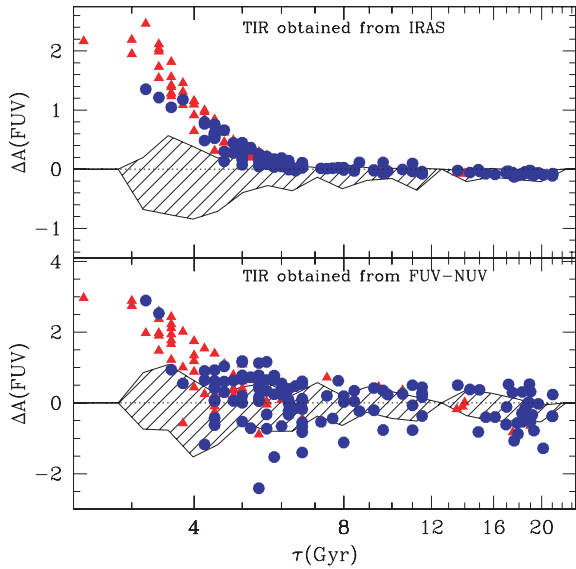


**Figure 6.** Residuals in the estimate of  $A(\text{FUV})$  obtained with the different methods described in Section 4. The TIR/FUV ratio is estimated using *IRAS* observations (upper panel) and the  $\text{FUV} - \text{NUV}$  colour (lower panel). The shaded areas show the typical uncertainties in the new recipes presented in this paper, estimated by generating 1000 random galaxies having  $\text{FUV} - H$  colour following a Gaussian distribution centred on the observed colour with  $\sigma = 0.2$  mag (see Section 4 for details). For comparison, the residuals obtained when an age-independent method is used are indicated by the filled symbols. The symbols are as in Fig. 3.

colour would correspond to a lower uncertainty on  $A(\text{FUV})$ ). For each  $\text{FUV} - H$  colour, the  $\tau$  PDFs are used to random generate the correspondent value of  $\tau^4$  and then the final value of  $A(\text{FUV})$  by applying the relations in Table 2. In Fig. 6 (upper panel), we compare this method with the SED-fitting technique. The shaded area indicates the  $1\sigma$  error on the estimate of  $A(\text{FUV})$ . As expected, the error on the estimate of  $A(\text{FUV})$  varies significantly with  $\tau$ : from  $\sim +0.1/-0.25$  mag for  $\tau \geq 6$  Gyr ( $\text{FUV} - H < 5$  mag) to a maximum of  $+0.4/-0.8$  mag for  $3.5 \leq \tau \leq 4.5$  Gyr ( $7 < \text{FUV} - H < 8.5$  mag). Even if the uncertainty for low  $\tau$  is quite large [due to the large variation of the TIR/FUV versus  $A(\text{FUV})$  relation with  $\tau$ ], it is clear that our empirical method is able to remove the systematic overestimate of  $A(\text{FUV})$  when the age-independent TIR/FUV versus  $A(\text{FUV})$  conversion is used (filled symbols in Fig. 6).

(ii) *FIR observations are not available.* In this case, the first step is to find a way to estimate the TIR/FUV ratio from the available observations. Recently, various methods have been proposed based on the use of the  $\text{FUV} - \text{NUV}$  colour (or  $\beta$ , Seibert et al. 2005; Cortese et al. 2006; Boissier et al. 2007; Gil de Paz et al. 2007),  $H$ -band luminosity (Cortese et al. 2006), gas metallicity (Cortese et al. 2006; Boissier et al. 2007), effective surface brightness (Cortese et al. 2006; Johnson et al. 2007a),  $D(4000)$  or optical and UV colours (Burgarella et al. 2005; Johnson et al. 2006, 2007a). Once the TIR/FUV ratio has been determined, it is possible to proceed as described above: that is, estimate  $\tau$  from an UV – optical/NIR colour (see Table 2) and then convert TIR/FUV in  $A(\text{FUV})$  using the proper relation in Table 1.

<sup>4</sup> This step is included in order to take into account the intrinsic dispersion of the  $\text{FUV} - H$  versus  $\tau$  relation in the estimate of  $\tau$ .

**Table 3.** The average value of  $A(\text{FUV})$  for our sample in bins of morphological type.

Type	$A(\text{FUV})$	$\sigma$
Sa	1.5	0.9
Sab	1.6	0.6
Sb	1.8	0.7
Sbc	1.8	0.6
Sc	1.5	0.6
Scd	1.2	0.8
Sd	0.9	0.6
Sm	1.5	0.4
Im-BCD	1.7	0.7

To test this second method we estimate the TIR/FUV ratio from the  $\text{FUV} - \text{NUV}$  colour (Cortese et al. 2006):

$$\log\left(\frac{\text{TIR}}{\text{FUV}}\right) = \begin{cases} 0.7(2.201 \text{FUV} - \text{NUV} - 1.804) + 1.3 & \text{if } (\text{FUV} - \text{NUV} \leq 0.9) \\ 1.424 & \text{if } (\text{FUV} - \text{NUV} > 0.9) \end{cases} \quad (10)$$

and then determine  $\tau$  from the  $\text{FUV} - H$  colour. The typical uncertainty in this method has been computed following the same procedure described in the previous point. Also in this case our recipe is able to remove the systematic overestimate on  $A(\text{FUV})$ . This is clearly evident in Fig. 6 (lower panel) where our method is compared with the age-independent method based on the  $\text{FUV} - \text{NUV}$  colour proposed by Salim et al. (2007). Unfortunately, the uncertainty on the determination of  $A(\text{FUV})$  considerably increases to  $\sim +0.5/-0.7$  mag for  $\tau \geq 6$  Gyr ( $\text{FUV} - H < 5$  mag) reaching a maximum of  $\sim +1/-1.2$  mag for  $3.5 \leq \tau \leq 4.5$  Gyr ( $7 < \text{FUV} - H < 8.5$  mag) when the total IR luminosity is estimated from empirical relations involving colours or luminosities. As discussed by Cortese et al. (2006) this is mainly due to the intrinsic scatter in the empirical relation used to determine the TIR/FUV ratio.

In the very unlikely scenario in which there is no sufficient data to estimate the TIR/FUV ratio and/or  $\tau$  as described above, the only possibility is to use the morphological type to obtain a rough estimate of  $A(\text{FUV})$ . In Table 3, we give the average value and standard deviation of  $A(\text{FUV})$  obtained for our sample in bins of morphological type. For our sample, this method provides an estimate of  $A(\text{FUV})$  with an average error of  $\sim 0.7$  mag. However, we recommend to apply this technique only when accurate an morphological classification is available (i.e. the local Universe), otherwise the error on  $A(\text{FUV})$  will be considerably larger than the one obtained for our sample.

## 5 IMPLICATIONS ON THE STUDY OF UV PROPERTIES OF GALAXIES

The simple recipes presented here have the widest scientific application possible, requiring only an UV and UV – optical colour. In order to show their real power, in the following we will discuss two different applications of these methods to the study of the UV properties of nearby galaxies and compare them with the age-independent techniques usually adopted.

### 5.1 Star formation density profiles of resolved galaxies

The *age effect* on the TIR/FUV versus  $A(\text{FUV})$  relation is particularly important in panchromatic studies of resolved galaxies

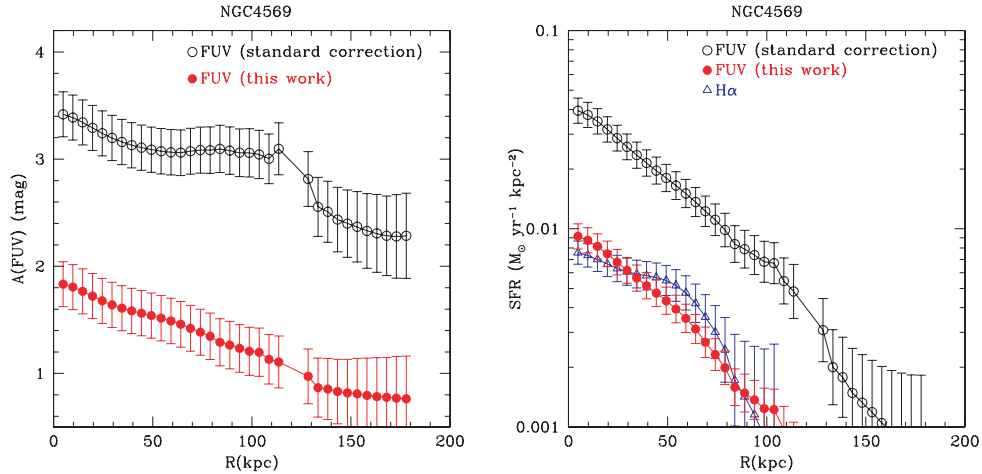


**Figure 7.** Left-hand panel: comparison between the FUV attenuation profile of NGC 4569 obtained following the standard TIR/FUV versus  $A(\text{FUV})$  conversion (empty circles) and the one obtained using the conversion presented in this work (filled circles). Right-hand panel: star formation rate density profile for NGC 4569. Star formation is obtained from the FUV corrected with the standard TIR/FUV versus  $A(\text{FUV})$  conversion (Buat et al. 2005) (empty circles), with the recipe presented in this work (filled circles) and from the  $H\alpha$  corrected for extinction using the Balmer decrement (empty triangles).

(Boissier et al. 2004, 2007; Calzetti et al. 2005; Pérez-González et al. 2006) since in different regions the dust can be heated up by different stellar populations (Calzetti et al. 2005).

We test our method on the nearby spiral galaxy NGC 4569 (M90), the brightest spiral galaxy in the Virgo cluster recently studied by Boselli et al. (2006). NGC 4569 can be considered as the prototype of  $H\text{I}$ -deficient galaxy having only about one-tenth of the atomic gas of a comparable field galaxy of similar type and size. This galaxy has a truncated  $H\alpha$  and  $H\text{I}$  radial profile (at a radius of  $\sim 5$  kpc, Cayatte et al. 1994; Koopmann & Kenney 2004; Boselli et al. 2006) and shows significant colour gradients with star formation activity only in the central 5 kpc. Therefore, given its significant age gradients, the contribution of UV photons to the dust heating probably varies with the distance from the galaxy centre, making this object ideal to compare with our recipes with age-independent techniques. As described in Boselli et al. (2006) we determined the TIR/FUV ratio profile combining *GALEX*-FUV image and *Spitzer* 24-, 70- and 160- $\mu\text{m}$  radial profiles. We then use the observed FUV –  $H$  colour profile to estimate  $\tau$  at each radius, determining which TIR/FUV versus  $A(\text{FUV})$  relation to use at each radius. The  $A(\text{FUV})$  profile so obtained is shown in Fig. 7 (left-hand panel, empty circles) and compared to the one estimated using the age-independent TIR/FUV versus  $A(\text{FUV})$  conversion (Buat et al. 2005). As expected, our method gives a FUV attenuation  $\sim 1.5$  mag lower than the standard conversion implying a factor of  $\sim 4$  difference in the SFR surface density profile obtained from the FUV profile (Fig. 7, right-hand panel). The results obtained with our technique are supported by the very good agreement with the SFR density profile independently obtained from the  $H\alpha$  line (corrected for extinction using Balmer decrement; Fig. 7 right-hand panel, empty triangles). In fact, only a recent ( $< 10^7$  yr) starburst  $\sim 100$  times stronger than the normal star formation rate in NGC 4569 could reconcile the difference between the SFR obtained from the  $H\alpha$  and from the FUV corrected with the standard methods (Iglesias-Páramo et al. 2004): an extremely unlikely scenario as discussed by Vollmer et al. (2004) and Boselli et al. (2006).

This exercise shows the crucial importance of the age-dependent TIR/FUV versus  $A(\text{FUV})$  relations in the panchromatic study of resolved galaxies.

## 5.2 The UV – optical colour–magnitude relation of large samples of galaxies

The need of empirical methods to correct for dust attenuation is particularly important for the study of UV properties of large samples of galaxies lacking FIR rest-frame data. Of particular importance for our understanding of galaxy evolution is the correct interpretation of the UV – optical colour–magnitude (CM) relation, as recently discussed by Wyder et al. (2007), Schiminovich et al. (2007) and Martin et al. (2007). It is very difficult to use a single correction technique able to deal simultaneously with starbursts, low SSFR objects and elliptical galaxies. Of particular importance is the correct estimate of  $A(\text{FUV})$  for transition objects: galaxies with low SSFR for which the standard corrections calibrated on active star-forming systems are likely to be not valid. In order to quantify the influence of the *age effect* on our interpretation of the UV – optical CM relation, we compare our method with the age-independent recipes using a sample of galaxies extracted from *GALEX* observations of the Coma cluster region (GI-Cycle 1, Cortese et al., in preparation). This sample includes all galaxies detected in both FUV and NUV bands as well as with SDSS-DR6 *ugriz* photometry and with spectroscopic redshift data available (833 galaxies). Since for this large sample FIR observations are not available, we use the second method described in Section 4, determining the TIR/FUV ratio from the FUV – NUV colour and  $\tau$  from the FUV –  $i$  colour. The FUV –  $r$  colour– $r$  magnitude relation obtained is compared with the observed one (i.e. not corrected for internal extinction) in Fig. 8 (left-hand panel). Whereas galaxies in the blue sequence (FUV –  $r \lesssim 4$  mag) have an average FUV dust attenuation  $A(\text{FUV}) \sim 1.5\text{--}2$  mag, galaxies in the red sequence (FUV –  $r \geq 6$  mag) show (as expected) a very low amount of attenuation ( $A(\text{FUV}) \sim 0.5$  mag) and occupy almost the same parameter space as uncorrected data. The separation between the red and blue sequences is therefore more evident after the correction for dust attenuation. We remark that our technique should not be blindly applied to elliptical galaxies, since in these objects UV emission comes from old stellar populations and not young stars (e.g. Boselli et al. 2005b). However, if an accurate morphological classification is not available the use of the recipes presented here does not introduce a strong

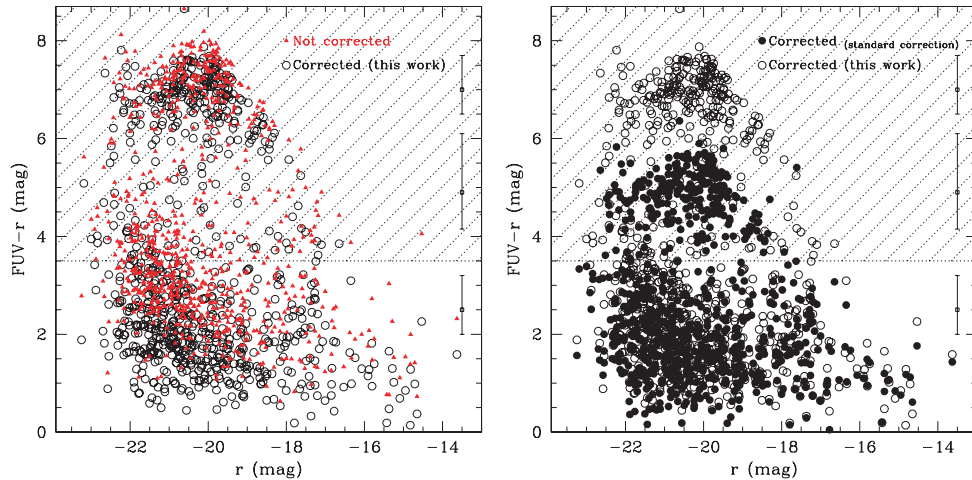


**Figure 8.** The  $FUV - r$  colour versus  $r$  magnitude relation for galaxies projected on the Coma cluster region. Left-hand panel: the triangles indicate the observed (i.e. not corrected for internal extinction) CM relation, while the empty circles show the CM relation after correcting for dust attenuation using the recipes presented in this work. Right-hand panel: the empty circles are as in the right-hand panel, whereas the filled circles show the CM relation obtained using the standard (i.e. age-independent) correction. The errors on the estimate of the corrected  $FUV - r$  for galaxies in the blue, red sequence and in the transition region are indicated by the empty squares. The unshaded regions indicate the range of observed (i.e. not corrected for internal extinction) colours on which the standard TIR/FUV versus  $A(FUV)$  relation for star-forming galaxies is usually calibrated.

systematic bias in the data, as shown in Fig. 8 (left-hand panel). This result indicates that our procedures are reliable for old as well as young stellar populations, contrary to previous empirical methods, calibrate and valid only for active star-forming galaxies (e.g. Johnson et al. 2006; Salim et al. 2007). This is clearly evident in Fig. 8 (right-hand panel) where the CM relation obtained with our recipe is compared with the one determined by using the age-independent method to convert the  $FUV - NUV$  colour into  $A(FUV)$  (e.g. Johnson et al. 2006; Salim et al. 2007). The difference between the two CM relations is quite impressive: while no significant difference is observed in blue-sequence galaxies, the red sequence shifts  $\sim 2$  mag towards bluer colours and the gap between the blue and red sequence (i.e. the so-called ‘green valley’, Wyder et al. 2007; Martin et al. 2007; Schiminovich et al. 2007) is considerably reduced. A similar result has been recently shown by Wyder et al. (2007) when comparing the CM relation determined using the Balmer decrement as an indicator of dust attenuation with the one estimated using the recipes proposed by Johnson et al. (2006). This result shows how strong the bias can be when blindly using the recipes to estimate  $A(FUV)$  without taking into account the *age effect*, leading to an incorrect interpretation of the data and reconstruction of galaxy’s evolution history.

## 6 CONCLUSIONS

We have investigated the dependence of the TIR/FUV versus  $A(FUV)$  relation on the average age of galaxy stellar populations. Our simple method has shown that even for spiral galaxies the use of a standard (i.e. not age-dependent) conversion of the TIR/FUV into  $A(FUV)$  leads to a systematic overestimate (i.e.  $\geq 1$  mag) of the dust attenuation in galaxies with low specific star formation, mainly anemic cluster spirals. This systematic bias strongly affects our interpretation of UV observations and can produce a significant overestimate (up to a factor of 10) of the star formation rate, particularly in H I-deficient galaxies. Therefore, we have developed different methods for determining the UV dust attenuation taking into account the age dependence of the TIR/FUV versus  $A(FUV)$

relation. These recipes require only an UV colour and an UV – optical/NIR colour providing an estimate of the UV attenuation with an average uncertainty varying from  $\sim +0.1/-0.25$  mag for  $\tau \geq 6$  Gyr ( $FUV - H < 5$  mag) to a maximum of  $+0.4/-0.8$  mag for  $3.5 \leq \tau \leq 4.5$  Gyr ( $7 < FUV - H < 8.5$  mag), when FIR observations are available, and from  $\sim +0.5/-0.7$  mag for  $\tau \geq 6$  Gyr ( $FUV - H < 5$  mag) to a maximum of  $\sim +1/-1.2$  mag for  $3.5 \leq \tau \leq 4.5$  Gyr ( $7 < FUV - H < 8.5$  mag) when FIR data are not available. The small amount of multiwavelength data necessary for their application makes these methods extremely useful for the widest possible range of application eventually providing us with a less biased view of the UV properties of galaxies in the local Universe and at higher redshift.

## ACKNOWLEDGMENTS

We want to thank the anonymous referee, whose comments and suggestions were extremely useful for improving this manuscript. We thank Jonathan Davies for useful discussions and comments on this manuscript. LC is supported by the UK Particle Physics and Astronomy Research Council. *GALEX* is a NASA Small Explorer, launched in 2003 April. We gratefully acknowledge NASA’s support for construction, operation, and science analysis for the *GALEX* mission, developed in cooperation with the Centre National d’Etudes Spatiales of France and the Korean Ministry of Science and Technology. This research has made use of the NASA/IPAC Extragalactic Data base, which is operated by the Jet Propulsion Laboratory, California Institute of Technology, under contract to NASA and of the GOLDMine data base

## REFERENCES

- Bianchi S., Ferrara A., Davies J. I., Alton P. B., 2000, MNRAS, 311, 601
- Binggeli B., Sandage A., Tammann G. A., 1985, AJ, 90, 1681
- Boissier S., Boselli A., Buat V., Donas J., Milliard B., 2004, A&A, 424, 465

- Boissier S., Gil de Paz A., Boselli A. et al., 2007, *ApJS*, 173, 524
- Boselli A., Gavazzi G., Donas J., Scodreggio M., 2001, *AJ*, 121, 753
- Boselli A., Gavazzi G., Sanvito G., 2003, *A&A*, 402, 37
- Boselli A., Boissier S., Cortese L. et al., 2005a, *ApJ*, 623, L13
- Boselli A., Cortese L., Deharveng J. M. et al., 2005b, *ApJ*, 629, L29
- Boselli A., Boissier S., Cortese L., Gil de Paz A., Seibert M., Madore B. F., Buat V., Martin D. C., 2006, *ApJ*, 651, 811
- Bruzual G., Charlot S., 2003, *MNRAS*, 344, 1000
- Buat V., 1992, *A&A*, 264, 444
- Buat V., Burgarella D., 1998, *A&A*, 334, 772
- Buat V., Xu C., 1996, *A&A*, 306, 61
- Buat V., Boselli A., Gavazzi G., Bonfanti C., 2002, *A&A*, 383, 801
- Buat V., Iglesias-Páramo J., Seibert M. et al., 2005, *ApJ*, 619, L51
- Burgarella D., Buat V., Iglesias-Páramo J., 2005, *MNRAS*, 360, 1413
- Burstein D., Heiles C., 1982, *AJ*, 87, 1165
- Calzetti D., 2001, *PASP*, 113, 1449
- Calzetti D., Kinney A. L., Storchi-Bergmann T., 1994, *ApJ*, 429, 582
- Calzetti D., Kennicutt J., R. C., Bianchi L. et al., 2005, *ApJ*, 633, 871
- Cayatte V., Kotanyi C., Balkowski C., van Gorkom J. H., 1994, *AJ*, 107, 1003
- Chabrier G., 2003, *PASP*, 115, 763
- Charlot S., Fall S. M., 2000, *ApJ*, 539, 718
- Cortese L., Boselli A., Buat V. et al., 2006, *ApJ*, 637, 242
- Dale D. A., Helou G., Contursi A., Silberman N. A., Kolhatkar S., 2001, *ApJ*, 549, 215
- Dale D. A., Gil de Paz A., Gordon K. D. et al., 2007, *ApJ*, 655, 863
- Disney M., Davies J., Phillipps S., 1989, *MNRAS*, 239, 939
- Donas J., Deharveng J.-M., Rich R. M. et al., 2007, *ApJS*, 173, 597
- Franzetti P., 2005, PhD thesis, Università degli Studi di Milano-Bicocca
- Franzetti P., Scodreggio M., Garilli B., Fumana M., Paioro L., 2008, in Lewis J., Argyle R., Bunclark P., Evans D., Gonzales-Solares E., eds, *ASP Conf. Ser. Vol., Astronomical Data Analysis Software and Systems XVII*. In press (astro-ph/0801.2518)
- Gallazzi A., Charlot S., Brinchmann J., White S. D. M., Tremonti C. A., 2005, *MNRAS*, 362, 41
- Gavazzi G., Boselli A., Scodreggio M., Pierini D., Belsole E., 1999, *MNRAS*, 304, 595
- Gavazzi G., Franzetti P., Scodreggio M., Boselli A., Pierini D., 2000, *A&A*, 361, 863
- Gavazzi G., Bonfanti C., Sanvito G., Boselli A., Scodreggio M., 2002, *ApJ*, 576, 135
- Gavazzi G., Boselli A., Donati A., Franzetti P., Scodreggio M., 2003, *A&A*, 400, 451
- Gil de Paz A., Boissier S., Madore B. F. et al., 2007, *ApJS*, 173, 185
- Gordon K. D., Clayton G. C., Witt A. N., Misselt K. A., 2000, *ApJ*, 533, 236
- Haynes M. P., Giovanelli R., 1984, *AJ*, 89, 758
- Heavens A., Panter B., Jimenez R., Dunlop J., 2004, *Nat*, 428, 625
- Helou G., Khan I. R., Malek L., Boehmer L., 1988, *ApJS*, 68, 151
- Iglesias-Páramo J., Boselli A., Gavazzi G., Zaccardo A., 2004, *A&A*, 421, 887
- Inoue A. K., Buat V., Burgarella D., Panuzzo P., Takeuchi T., Iglesias-Páramo J., 2006, *MNRAS*, 370, 380
- Johnson B. D., Schiminovich D., Seibert M. et al., 2006, *ApJ*, 644, L109
- Johnson B. D., Schiminovich D., Seibert M., et al. 2007a, *ApJS*, 173, 377
- Johnson B. D., Schiminovich D., Seibert M., et al. 2007b, *ApJS*, 173, 392
- Kennicutt R. C., Tamblyn P., Congdon C. E., 1994, *ApJ*, 435, 22
- Kong X., Charlot S., Brinchmann J., Fall S. M., 2004, *MNRAS*, 349, 769
- Koopmann R. A., Kenney J. D. P., 2004, *ApJ*, 613, 866
- Martin D. C., Fanson J., Schiminovich D. et al., 2005, *ApJ*, 619, L1
- Martin D. C., Wyder T. K., Schiminovich D. et al., 2007, *ApJS*, 173, 342
- Meurer G. R., Heckman T. M., Leitherer C., Kinney A., Robert C., Garnett D. R., 1995, *AJ*, 110, 2665
- Meurer G. R., Heckman T. M., Calzetti D., 1999, *ApJ*, 521, 64
- Panter B., Jimenez R., Heavens A. F., Charlot S., 2007, *MNRAS*, 378, 1550
- Panuzzo P., Bressan A., Granato G. L., Silva L., Danese L., 2003, *A&A*, 409, 99
- Panuzzo P., Granato G. L., Buat V., Inoue A. K., Silva L., Iglesias-Páramo J., Bressan A., 2007, *MNRAS*, 375, 640
- Pei Y. C., 1992, *ApJ*, 395, 130
- Pérez-González P. G., Kennicutt J., R. C., Gordon K. D. et al., 2006, *ApJ*, 648, 987
- Piovan L., Tantaló R., Chiosi C., 2006, *MNRAS*, 370, 1454
- Popescu C. C., Tuffs R. J., 2002, *MNRAS*, 335, L41
- Salim S., Rich R. M., Charlot S. et al., 2007, *ApJS*, 173, 267
- Salpeter E. E., 1955, *ApJ*, 121, 161
- Sauvage M., Thuan T. X., 1992, *ApJ*, 396, L69
- Schiminovich D., Wyder T. K., Martin D. C. et al., 2007, *ApJ*, 173, 315
- Seibert M., Martin D. C., Heckman T. M. et al., 2005, *ApJ*, 619, L55
- Silva L., Granato G. L., Bressan A., Danese L., 1998, *ApJ*, 509, 103
- Vollmer B., Balkowski C., Cayatte V., van Driel W., Huchtmeier W., 2004, *A&A*, 419, 35
- Walterbos R. A. M., Greenawalt B., 1996, *ApJ*, 460, 696
- Witt A. N., Gordon K. D., 2000, *ApJ*, 528, 799
- Wyder T. K., Martin D. C., Schiminovich D. et al., 2007, *ApJS*, 173, 293
- Xu C., Buat V., 1995, *A&A*, 293, L65
- Zwicky F., Herzog E., Wild P., 1961, *Catalogue of Galaxies and of Clusters of Galaxies*. California Institute of Technology (CIT), Pasadena

## APPENDIX A: THE DEPENDENCE OF THE TIR/FUV VERSUS $A(FUV)$ RELATION ON EXTINCTION LAW, DUST GEOMETRY AND SFH

Are the results obtained in this work and the recipes proposed to estimate the UV dust attenuation model-dependent? In order to answer to this question, in this section we investigate the dependence of our results on the three free parameters entering our model: the shape of the extinction law, the dust geometry and the SFH.

In Fig. A1 (left-hand panel), we show the TIR/FUV versus  $A(FUV)$  relation obtained for different values  $\tau$ , a Sandwich geometry and three different extinction laws: LMC (solid line), MW (dotted line) and Small Magellanic Cloud (dashed line). As already pointed out by several authors (e.g. Witt & Gordon 2000; Buat et al. 2005), the TIR/FUV versus  $A(FUV)$  relation is almost independent of the extinction law with a typical variation limited to  $\leq 0.2$  mag, considerably lower than the effect of  $\tau$  on the TIR/FUV versus  $A(FUV)$  relation.

Similar results are obtained if we investigate the effect of different dust geometries. In Fig. A1 (right-hand panel), we compare the results obtained for the sandwich model (solid line) with a simple slab geometry (Disney, Davies & Phillipps 1989, dashed line). We also added the results for a Calzetti, Kinney & Storchi-Bergmann (1994) attenuation law (dotted line). Even in this case, we observed no dependence of the TIR/FUV versus  $A(FUV)$  relation on the dust geometry within  $\leq 0.2$  mag. Similar results are obtained if we use the homogeneous and clumpy dust models proposed by Witt & Gordon (2000) (not shown).

Finally, we fitted the 191 galaxies in our sample with various SED libraries in order to test the dependence of the results presented in Sections 3 and 4 from SFH and age. The SED library used in Section 2 has been obtained by fixing the shape of the SFH (assumed to be ‘a la Sandage’), the age of the galaxy (assumed equal to 13 Gyr) and the stellar IMF (assumed to be a Salpeter IMF). We produced different set of SED libraries varying every time one of these three free parameters and we fitted them to the data. In particular, we considered an exponential SFH, a fixed ( $t = 13$  Gyr) or free (in the range  $0 < t < 15$  Gyr) age and a Chabrier (2003) IMF. In Fig. A2, the difference in the estimate of  $A(FUV)$  between the library

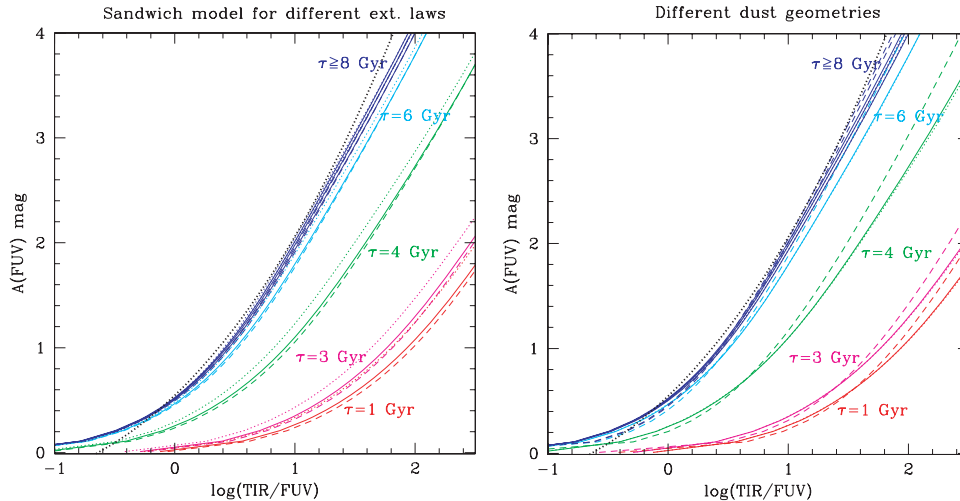


**Figure A1.** The relationship between the TIR/FUV ratio and the FUV attenuation  $A(\text{FUV})$  obtained from our model using different extinction laws and geometries. Left-hand panel: sandwich geometry with LMC (solid line), MW (dashed line) and Small Magellanic cloud (dotted line) extinction laws. Right-hand panel: LMC extinction law with sandwich (solid line), simple slab (dotted) geometries and Calzetti attenuation law (dashed line). In both panels, the dotted black line indicates the age-independent relation given by Buat et al. (2005).

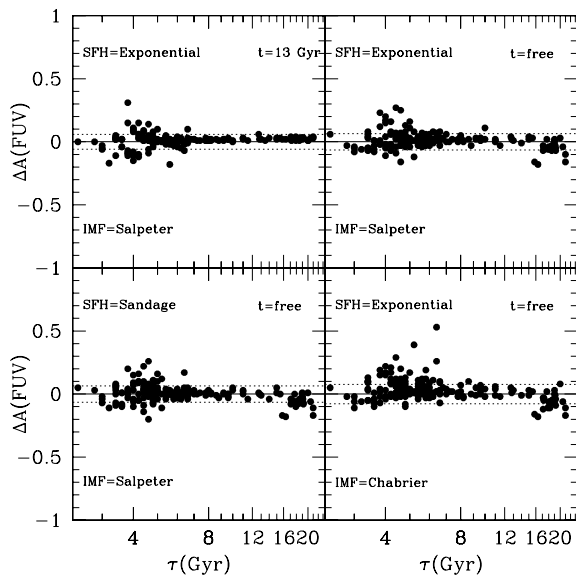


**Figure A2.** Difference in the estimate of  $A(\text{FUV})$  with the SED technique described in Section 3 ( $t = 13$  Gyr, ‘a la Sandage’ SFH and Salpeter IMF) and various combinations of SFHs (Sandage or exponential), age (variable or fixed to 13 Gyr) and IMF (Salpeter or Chabrier). The dashed lines indicate the  $1\sigma$  difference in the estimate of  $A(\text{FUV})$ .

adopted in Section 2 and some of the various combination adopted is presented. For each combination, the standard deviation in the estimate of  $A(\text{FUV})$  is lower than 0.1–0.2 mag. This result was somehow expected since the TIR/FUV versus  $A(\text{FUV})$  relation is only affected by the actual shape of the SED and not by the shape of the past (older than 1–2 Gyr) SFH. We remark that our results are not applicable only in the case of an embedded starburst in a galaxy with a second older, less-embedded stellar population (Gordon et al. 2000). At UV and IR wavelengths, the starburst would dominate, but at optical and NIR wavelengths the older population would dominate. However, at least for spiral galaxies in the local Universe this seems not to be the case (Iglesias-Páramo et al. 2004) and smooth SFH

like ‘a la Sandage’ and exponential well reproduce the observations (e.g. Boselli et al. 2001; Gavazzi et al. 2002; Heavens et al. 2004; Panter et al. 2007)

We can therefore conclude that the results obtained from our model and the recipes presented in this work are model-independent at least within  $\sim 0.2$  mag. This uncertainty is still lower or equal to the uncertainty in the estimate of  $A(\text{FUV})$  from our recipes.

## APPENDIX B: RECIPES TO DETERMINE $A(\text{NUV})$ WHEN FUV OBSERVATIONS ARE NOT AVAILABLE

In this appendix, we discuss the possibility to extend our recipes to the NUV band in the case that *GALEX*-FUV observations are available. The *GALEX*-NUV filter ( $\lambda_{\text{eff}} = 2310 \text{ \AA}$ ,  $\Delta\lambda = 1000 \text{ \AA}$ ) lies in a region where the SED of galaxies with  $\tau < 4$  Gyr is strongly dependent on stellar metallicity for  $Z > 0.2 Z_{\odot}$  (e.g. see fig. 6 in Gavazzi et al. 2002). This strongly affects the TIR/NUV versus  $A(\text{NUV})$  relation which, for low values of  $\tau$ , can vary by even 0.4 mag from  $Z = 0.2$  to  $0.02 Z_{\odot}$ , apparently complicating the use of our model directly on the NUV band. However, for none of the galaxies with  $\tau < 4$  Gyr in our sample the best-fitting model has metallicity lower than  $Z = 0.2 Z_{\odot}$ , consistent with the fact that in the local Universe evolved galaxies tend to be metal-rich (e.g. Gallazzi et al. 2005). Therefore, for  $\tau < 4$  Gyr we compute the average TIR/NUV versus  $A(\text{NUV})$  relation by combining only the relations obtained in the metallicity range  $0.02 < Z < 2.5 Z_{\odot}$ . This makes our recipes not valid for  $\tau < 4$  Gyr and  $Z < 0.2 Z_{\odot}$ . The average TIR/NUV versus  $A(\text{NUV})$  relations for different values of  $\tau$  so obtained are presented in Table B1. In Table B2, the relations to use to estimate  $\tau$  from the NUV – optical/NIR colours are given. Their typical dispersion is consistent with the one observed in the FUV – optical/NIR colours versus  $\tau$  relations. As discussed in Section 4, the suggested recipes to determine  $A(\text{NUV})$  are as follows.

(i) *FIR observations are available.* We determine the observed TIR/NUV ratio and use one of the relations presented in Table B2 to determine  $\tau$ . Finally, we use the value of  $\tau$  obtained with this procedure to choose the conversion between the TIR/FUV ratio

**Table B1.** Relations to convert the TIR/NUV ratio in  $A(\text{NUV})$  for different values of  $\tau$  and  $\text{NUV} - \text{NIR/optical}$  colours.

$\tau$ (Gyr)	$A(\text{NUV}) = (a1) + (a2)x + (a3)x^2 + (a4)x^3 + (a5)x^4$ , where $x = \log(\text{TIR/NUV})$					$\text{NUV} - H$	$\text{NUV} - i$	$\text{NUV} - r$	$\text{NUV} - g$	$\text{NUV} - B$
	$a1$	$a2$	$a3$	$a4$	$a5$					
$\leq 2.6$	0.04030	0.12924	0.02301	0.14889	-0.01909	9.3	6.2	5.9	5.3	5.0
2.8	0.04436	0.13118	0.03649	0.14669	-0.01911	8.9	5.9	5.6	5.0	4.7
3	0.05370	0.13840	0.06591	0.14195	-0.01921	8.5	5.5	5.3	4.7	4.4
3.2	0.07037	0.15838	0.11195	0.13508	-0.01962	8.2	5.2	5.0	4.5	4.2
3.4	0.09423	0.19557	0.16580	0.12827	-0.02060	7.9	4.9	4.7	4.2	3.9
3.6	0.12309	0.24566	0.21875	0.12335	-0.02236	7.5	4.6	4.5	4.0	3.7
3.8	0.15343	0.30012	0.26696	0.12089	-0.02490	7.3	4.4	4.2	3.8	3.5
4	0.18195	0.35210	0.30967	0.12051	-0.02805	7.0	4.1	4.0	3.6	3.3
4.2	0.21793	0.41714	0.35825	0.11985	-0.03139	6.7	3.9	3.8	3.4	3.1
4.4	0.23640	0.45238	0.38817	0.12220	-0.03488	6.5	3.7	3.5	3.2	2.9
4.6	0.25119	0.48147	0.41412	0.12486	-0.03822	6.2	3.5	3.3	3.0	2.7
4.8	0.26292	0.50518	0.43641	0.12761	-0.04131	6.0	3.2	3.1	2.9	2.5
5	0.27220	0.52449	0.45540	0.13025	-0.04406	5.8	3.0	3.0	2.7	2.3
5.4	0.28548	0.55319	0.48523	0.13492	-0.04854	5.3	2.7	2.6	2.4	2.0
5.8	0.29415	0.57274	0.50686	0.13873	-0.05189	5.0	2.3	2.3	2.1	1.7
6.2	0.30003	0.58647	0.52278	0.14176	-0.05439	4.6	2.0	2.0	1.8	1.5
6.6	0.30418	0.59643	0.53473	0.14418	-0.05626	4.3	1.7	1.7	1.6	1.2
7	0.30720	0.60385	0.54390	0.14613	-0.05770	3.9	1.4	1.4	1.3	1.0
$\geq 8$	0.31194	0.61587	0.55922	0.14955	-0.06009	$< 3.6$	$< 1.1$	$< 1.2$	$< 1.1$	$< 0.8$

Note. Each value of  $\tau$  has been converted into  $\text{NUV} - \text{NIR/optical}$  colours using the relations presented in Table B2.

**Table B2.** Linear relations useful to estimate  $\tau$  from observed (i.e. not corrected for dust attenuation)  $\text{NUV} - \text{NIR/optical}$  colours [ $\log(\tau) = ax + b$ ]. These relations have been calibrated and are valid only in the range  $2 \leq \tau \leq 7$  Gyr.

$x$	$a$	$b$	$r$	Validity range
$\text{NUV} - H$	-0.080	1.16	-0.88	$4.0 \lesssim \text{NUV} - H$
$\text{NUV} - i$	-0.089	0.97	-0.88	$1.5 \lesssim \text{NUV} - i$
$\text{NUV} - r$	-0.095	0.98	-0.88	$1.5 \lesssim \text{NUV} - r$
$\text{NUV} - g$	-0.108	0.99	-0.89	$1.5 \lesssim \text{NUV} - g$
$\text{NUV} - B$	-0.107	0.95	-0.90	$1.0 \lesssim \text{NUV} - B$

and  $A(\text{FUV})$  from the relations provided in Table B1. The typical error on the estimate of  $A(\text{NUV})$  (computed through a Monte Carlo simulation similar to the one described in Section 4) varies between  $\sim +0.1/-0.2$  mag for  $\tau \geq 8$  Gyr, to  $+0.3/-0.7$  mag for  $3.5 \leq \tau \leq 4.5$  Gyr.

(ii) *FIR observations are not available.* In this case, the first step is to find a way to determine the TIR/NUV from the observations available. Once the TIR/NUV ratio has been determined, it is sufficient to proceed as described in the previous point: that is, we estimate  $\tau$  from an UV - optical/NIR colour and then convert TIR/NUV in  $A(\text{NUV})$  using the proper relation in Table B1. The typical error on the estimate of  $A(\text{NUV})$  (computed through a Monte Carlo simulation similar to the one described in Section 4)

**Table B3.** The average value of  $A(\text{NUV})$  for our sample in bins of morphological type.

Type	$A(\text{NUV})$	$\sigma$
Sa	1.2	0.7
Sab	1.3	0.5
Sb	1.4	0.6
Sbc	1.4	0.5
Sc	1.2	0.5
Scd	0.9	0.7
Sd	0.8	0.5
Sm	1.2	0.3
Im-BCD	1.3	0.6

varies between  $\sim +0.4/-0.6$  mag for  $\tau \geq 8$  Gyr, and to  $\sim +0.9/-1$  mag for  $3.5 \leq \tau \leq 4.5$  Gyr.

In Table B3, the average values of  $A(\text{NUV})$  obtained for the different morphological types in our sample are presented. The morphological type can be used to estimate  $A(\text{NUV})$  only if the previous methods cannot be applied and an accurate morphological classification is available.

This paper has been typeset from a  $\text{T}_{\text{E}}\text{X}/\text{L}_{\text{A}}\text{T}_{\text{E}}\text{X}$  file prepared by the author.